Solid–Liquid Equilibria in 1,8-Cineole/Terpenic Hydrocarbon Systems

Aquiles Gomes, Lurdes Serrano, and Fátima Farelo*

Department of Chemical Engineering, Technical University of Lisbon, 1096 Lisboa Codex, Portugal

Solid–liquid phase diagrams have been obtained (at 1 atm pressure) for the binary systems 1,8-cineole/(−)-α-pinene, 1,8-cineole/(+)-limonene, and (−)-α-pinene/(+)-limonene. The polythermal projection of the liquidus surfaces was chosen to describe the phase diagram of the ternary terpenic system, where an invariant point was identified.

Introduction

1,8-Cineole is a chemical with several pharmaceutical applications, obtainable from rectified eucalyptus oil by batch crystallization. Though solid–liquid equilibrium (SLE) data for this multicomponent system are not available, good predictions can be achieved if the SLE for the ternary system 1,8-cineole ($C_{10}H_{18}O$)/(−)-α-pinene ($C_{10}H_{16}$)/(+)-limonene ($C_{10}H_{16}$) is known, since these three chemicals represent over 99% of the rectified eucalyptus oil.

In this work, the solid–liquid diagrams for the three binary systems 1,8-cineole/(−)-α-pinene, 1,8-cineole/(+)-limonene, and (−)-α-pinene/(+)-limonene and for the ternary system were obtained over the entire range of composition, at 1 atm pressure.

To our knowledge, no data on these systems were previously reported.

Experimental Section

Chemicals. Analytical grade (−)-α-pinene (99+ mol %) was purchased from Fluka, and the two main impurities (camphene and β-pinene) were identified. (+)-Limonene supplied by Cirel, Portugal, was 99.4+ mol %, the balance being γ-terpinene. Technical grade 1,8-cineole was purchased from BDH and further purified by zone melting in a multizone Desaga apparatus, the runs being carried out below room temperature. The mole percentage of impurities (mainly α-pinene) in the final purified cineole was 0.1, determined by the standard *o*-cresol method and checked via gas chromatography.

Prior to use, these chemicals were dried for at least 24 h at room temperature with potassium aluminiosilicate 1/16-in. pellets molecular sieve.

Apparatus and Procedure. Solutions were prepared by weighing directly the dried chemicals to ±0.1 mg, into screw-capped Pyrex tubes.

The freezing point apparatus was of conventional type (*1*) consisting of a 1.5 × 17 cm Pyrex tube, sealed in a double-walled glass jacket, with the outer chamber connected to a vacuum line. The Pt resistance thermometer sat in a well that went down through the center of the freezing tube and was coupled to a high-precision Digitron recorder. The Pt resistance thermometer (Digitron Inst.) was calibrated to IPTS-1968 scale over the range 73–293 K and estimated to be accurate to ±0.03 K.

Stirring was accomplished by a motor-driven stainless steel coil that moved vertically in the freezing cell at 100 strokes/min. Precautions were taken to prevent condensation of moisture into the samples.

For low-temperature measurements (below 223 K), liquid nitrogen was used as the coolant. For higher temperatures we used a thermostated bath, Hectofrig flow cooler, with precise temperature control and strong agitation.

Table I. Solid–Liquid Phase Equilibria in 1,8-Cineole Binary Systems[a]

x	T, K	x	T, K	x	T, K
1,8-Cineole/(−)-α-Pinene					
0	218.39[b]	0.0984	199.29	0.2746	225.56
0.0088	216.82	0.1075	196.77	0.4690	245.89
0.0177	214.96	0.1166	193.54	0.6733	258.54
0.0444	209.82	0.1257	196.60	0.8883	270.32
0.0894	201.50	0.1348	200.23	1.0000	274.63[b]
1,8-Cineole/(+)-Limonene					
0	198.65[b]	0.0623	190.28	0.2746	227.50
0.0071	197.92	0.0894	184.05	0.3706	236.52
0.0106	197.49	0.0984	191.20	0.5699	252.41
0.0266	195.80	0.1166	200.06	0.7794	264.58
0.0444	192.74	0.1809	215.53	1.0000	274.63[b]

[a] x values are mole fraction of 1,8-cineole and T melting temperatures. [b] Corrected to zero impurity.

All transfers of material between the screw-capped Pyrex tubes and the freezing tube were made with syringes to reduce evaporation losses.

Time–temperature warming curves were used to obtain liquidus temperatures. The determinations were made using quickly frozen samples thus ensuring an homogeneous distribution of the components in the initial solid (*2*, *3*).

Liquidus lines were checked under microscopic observation, down to 230 K. We used a modified Leitz microscope where the usual stage was replaced by a thermostated one. The recirculating fluid was refrigerated by the Hectofrig cooling unit previously referred to. The microscope stage was heated by a voltage-controlled resistance and was equipped with a Pt resistance thermometer coupled to a high-precision recorder. A moisture-free environment was created around the stage by the circulation of cold nitrogen. Agreement between the two methods was usually within ±0.05 K.

Cooling curves were not considered suitable for melting point determination. Extrapolation of time–temperature curves across the undercooling region produces a deviation of the actual liquidus from ±0.1 K (at 294 K) to ±5 K (at 110 K), when the increase in viscosity causes serious troubles.

The freezing temperatures of the pure chemicals were corrected to zero impurities. The accuracies of these temperatures and those of the eutectic temperatures of the 1,8-cineole systems are estimated to be ±0.05 and ±0.5 K, respectively.

For the terpenic binary (−)-α-pinene/(+)-limonene, as well as for the lower part of the ternary diagram (up to 10% of 1,8-cineole), ternary eutectic temperature being included, we evaluate the measurements accuracy to be no better than ±2.5 K.

Results

Table I summarizes the melting temperatures of the 1,8-cineole binary systems. For the 1,8-cineole/(−)-α-pinene system we observe (Figure 1) an eutectic point at 193.3 K and 0.1184 mole fraction of cineole. The 1,8-cineole/(+)-limonene system shows (Figure 2) the same type of solid–liquid phase diagram but the eutectic occurs at 182.5 K and mole fraction 0.0930 of 1,8-cineole.

Table II reports liquidus and solidus temperatures of the (−)-α-pinene/(+)-limonene system. The resulting phase diagram, shown in Figure 3, exhibits an eutectic point at 111.9 K

0021-9568/88/1733-0194$01.50/0

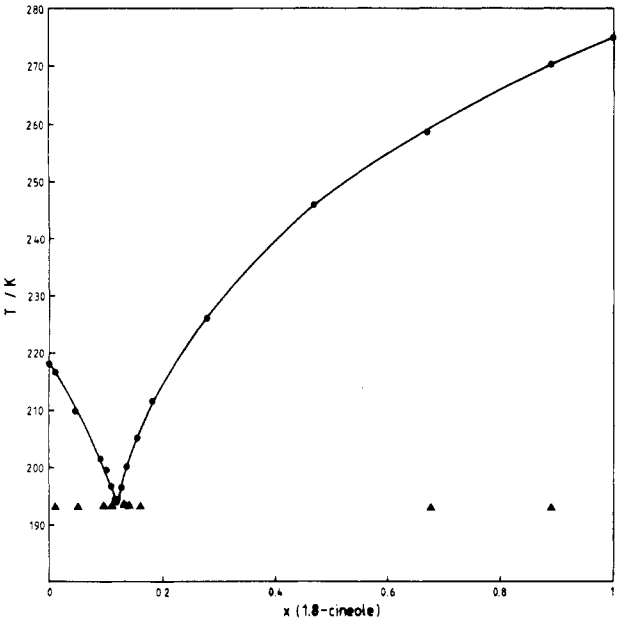

Figure 1. Solid–liquid phase diagram for the 1,8-cineole/(−)-α-pinene system.

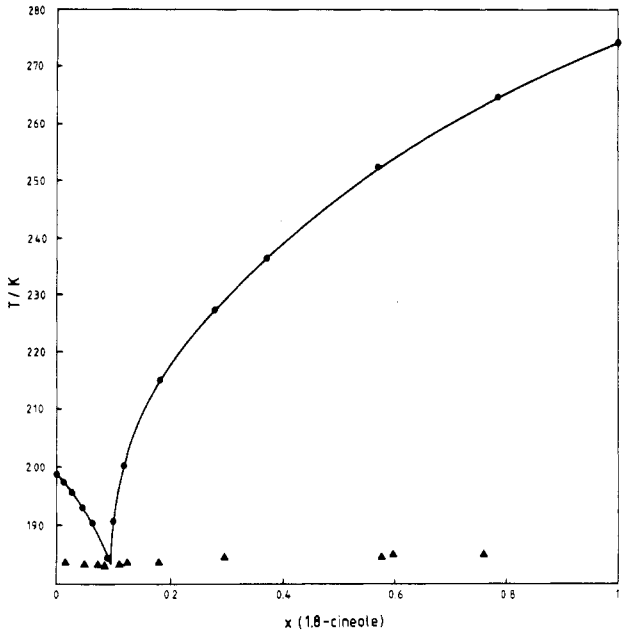

Figure 2. Solid–liquid phase diagram for the 1,8-cineole/(+)-limonene system.

Table II. Solid-Liquid Phase Diagram for the System (−)-α-Pinene/(+)-Limonene

x^a	T,[b] K	x^a	T,[b] K	x^a	T,[b] K
0	198.65[c]	0.2875	132	0.6940	184
0.0531	190	0.3089	126	0.7578	196
	165[d]	0.3208	118		118[d]
0.1038	177	0.3596	124	0.8066	199
	134[d]	0.4101	136		135[d]
0.1554	170	0.4895	151	0.9037	210
0.2068	157	0.6100	172		171[d]
0.2579	142			1.0000	218.39[c]

[a] x values are mole fraction of (−)-α-pinene. [b] T represents melting temperatures. [c] Corrected to zero impurities. [d] Solidus points.

and mole fraction 0.3259 (−)-α-pinene. Solid solubility is evident on both sides of the eutectic point with a rather large miscibility gap. The determination of solvus lines required very low temperatures, and repeatability was below acceptable values

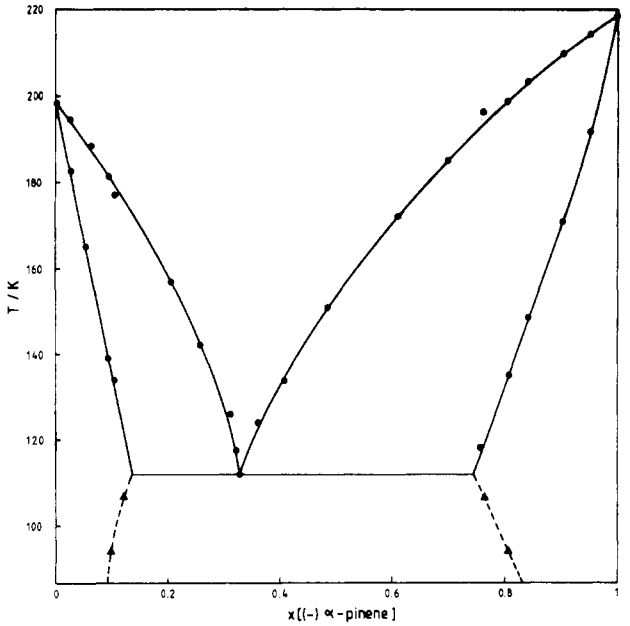

Figure 3. Solid–liquid phase diagram for the (−)-α-pinene/(+)-limonene system.

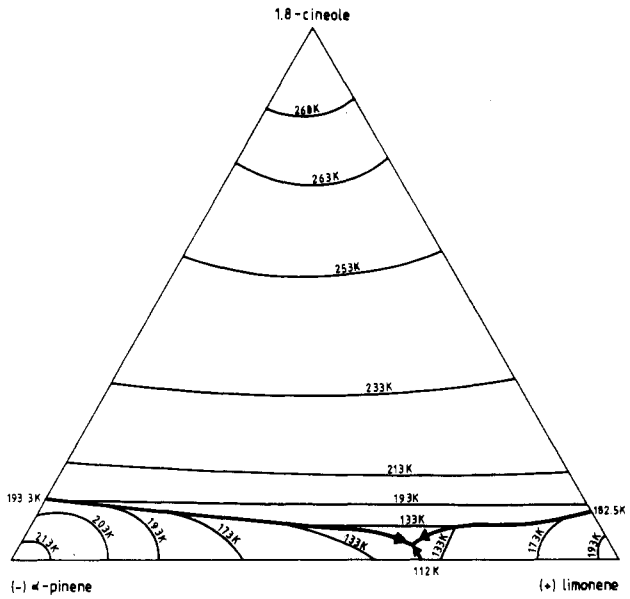

Figure 4. Phase diagram for the ternary system

Table III. Internal Section: Characteristic Points in the Ternary System

starting binary	mole fraction of (−)-α-pinene	3rd compd added	x^a	T, K	x^a	T, K
α-pinene/(+)-limonene	0.9789	1,8-cineole	0.1106	192		
	0.8534		0.1004	189		
	0.7548		0.0844	177		
	0.6322		0.0782	164		
	0.5089		0.0579	124		
	0.3825		0.0487	115		
	0.3206		0.0370	105		
	0.2010		0.0663	153		
	0.1115		0.0725	162		
	0.0423		0.0829	181		
1,8-cineole/α-pinene	0.8012	(+)-limonene	0.6998	133		
	0.8489		0.6731	113		
	0.9046		0.6552	108	0.6124	105
	0.9478		0.6749	110		

[a] Mole fraction in the ternary mixture of third component added.

(solvus lines only shown as dashed lines in Figure 3).

These three binary diagrams depict sides of a right triangular prism chosen to describe the temperature–composition relationships in the ternary system. A polythermal projection on the composition plane was adopted to describe the liquidus surfaces of the ternary system (Figure 4).

The eutectic valleys were found by measuring the solid–liquid equilibria along internal sections of the ternary diagram (*4*). Some characteristic points are listed in Table III.

The ternary system shows an invariant eutectic point at 102 K, with composition (in mole fraction) 0.287 1,8-cineole, 0.325 (–)-α-pinene, such composition having been estimated by perspective projections of the eutectic valleys (*5*).

In summary, Figure 4 shows that from the viewpoint of 1,8-cineole production more than 80% of the area of the ternary diagram can be used, thus exceeding by far the range of temperatures available for industrial purposes. In this study, low-temperature determinations were made difficult by glass-type transitions (whenever the increase in viscosity prevented stirring), which were responsible for the decrease in accuracy as temperature was lowered.

Registry No. 1,8-Cineole, 470-82-6; (+)-limonene, 5989-27-5; (–)-α-pinene, 7785-26-4.

Literature Cited

(1) Goates, J. R.; Ott, J. B.; Budge, A. H. *J. Phys. Chem.* **1961**, *65*, 2162.
(2) van Wijk, H. F.; Smit, W. M. *Anal. Chim. Acta* **1960**, *23*, 545.
(3) van Wijk, H. F.; Smit, W. M. *Anal. Chim. Acta* **1961**, *24*, 41.
(4) Tamás, F.; Pál, I. *Phase Equilibria Spatial Diagrams*, 1st ed.; Butterworth: Budapest, 1970; Chapter III.
(5) Ricci, J. E. *The Phase Rule* and *Heterogeneous Equilibrium*; Dover: New York, 1966; p 315.

Received for review December 29, 1986. Accepted October 26, 1987. This work was sponsored by the Instituto Nacional de Investigação Científica and by Fundação Calouste Gulbenkian, Portugal. We thank Cirel, L. Pastora, Portugal, for kindly supplying the (+)-limonene used in this work.

Effect of Pressure on the Constant-Pressure Heat Capacity of a Methane–Carbon Dioxide Mixture

James R. Boulton and Fred P. Stein*

Chemical Engineering Department, Lehigh University, Bethlehem, Pennsylvania 18015

The constant-pressure heat-capacity ratio, $C_{p\,HP}/C_{p\,1atm}$ (where $C_{p\,HP}$ is the heat capacity at high pressure and $C_{p\,1atm}$ the heat capacity at 1 atm), was measured for a 49.2 mol % mixture of methane in carbon dioxide along isotherms of 302.2, 312.7, and 325.2 K at pressures between 7 and 60 bar. No maximum in the heat capacity was encountered. The largest heat-capacity ratio (1.399, 1.340, and 1.263 for each isotherm, respectively) occurred at 60 bar. The uncertainty in the heat-capacity ratios is estimated to be 0.6%. The data were compared to heat-capacity ratios calculated from the Soave–Redlich–Kwong equation of state.

Introduction

Wherever nonidealities are significant in an energy balance applied to the design and analysis of process equipment, ideal-gas heat capacities are used in conjunction with enthalpy departures calculated from an equation of state (EOS). Even if constant-pressure heat capacities (C_p) for gases at high pressure were available, it is unlikely that they would be used directly in such process analysis. However, high-pressure C_p's would be very valuable for adjusting the parameters in the EOS subsequently used in the process analysis.

The direct calorimetric measurement of C_p at high pressure is a very difficult task, which explains the paucity of such data, but the measurement of the ratio of C_p at high pressure to C_p at 1 atm is, *relatively* speaking, easy. We have adopted the heat-exchange method for measuring the C_p ratio. This method was first used by Workman (*1*, *2*) in 1930 for oxygen, nitrogen, and hydrogen. Interest in the Workman calorimeter was revived in 1970 by Balaban and Wenzel (*3*) who studied nitrogen–trifluoromethane mixtures. Shortly thereafter, Bishnoi and Robinson (*4*, *5*) reviewed the available equipment and used the Workman calorimeter to study carbon dioxide–methane mixtures. Bishnoi et al. (*6*) and Hamaliuk et al. (*7*) studied nitrogen–carbon dioxide mixtures and nitrogen–hydrogen sulfide mixtures, respectively.

In the Workman calorimeter, the C_p ratio can be measured without measuring the flow rate (or mass) of the gas and without worrying about the heat leak, or its size, as long as it is reasonably small. The C_p at high pressure, then, is readily available because the C_p at 1 atm is known for many materials, or, for a mixture, it can be calculated from the ideal-gas C_p's of the constituents.

The difference between a high-pressure C_p and the ideal-gas C_p at the same temperature is related to the pressure–volume–temperature (PVT) properties of the gas, that is, related to an EOS. Thus, the data presented here afford an opportunity to test different aspects of an EOS than the usual tests provided by $P-V-T$ and vapor–liquid equilibrium measurements. We elected to compare calculations of the C_p ratio from the Soave–Redlich–Kwong EOS to the data.

Experimental Section

Materials. The gas mixture used in these experiments was 49.2 ± 0.4 mol % methane in carbon dioxide, as determined by gas chromatographic (GC) analysis using composition standards traceable to the U.S. National Bureau of Standards. GC analysis which focused on the impurities showed 14 ppm (molar) ethane and about 0.7 ppm ethylene. Periodically during the measurements, samples were removed from the apparatus and checked by GC for any air that may have contaminated the test gas during loading or operation. No air was detected in any of the samples; the limit of detectability was 0.05%.

Apparatus. The method used for experimentally determining the Cp ratios in the form $C_{p\,HP}/C_{p\,1atm}$ was first used by Workman (*1*). A schematic of the apparatus is shown in Figure 1; the details are available elsewhere (*8*).

The measurements were made in the countercurrent-flow heat exchanger in which the test gas passes through one side at high pressure and through the other side at 1 atm. Because

0021-9568/88/1733-0196$01.50/0